CO_2 Assisted Ethane Oxidative Dehydrogenation Over MoO_3 and V_2O_5 catalysts supported on Reducible CeO_2-TiO_2

Thu D. Nguyen, Fuat E. Celik and George Tsilomelekis**

Department of Chemical and Biochemical Engineering, Rutgers, The State University of New Jersey, Piscataway, NJ 08854, USA.

KEYWORDS: Lattice oxygen, Operando Raman Spectroscopy, Molybdena, Vanadia, Mixed metal oxides

ABSTRACT

Supported MO_x (M= Mo, V) on mixed CeO_2-TiO_2 were investigated for the oxidative dehydrogenation of ethane (ODHE) using CO_2 as a mild oxidant. Raman spectroscopic characterization of the synthesized catalysts under dehydrated conditions suggest that surface MoO_x species prefer to anchor on the crystalline domains of TiO_2. Upon increasing the amount of CeO_2 in the mixed oxide support, an intense and broad band at ~930cm^{-1} underscored that the prevalent species tend to be polymeric $(MoO_x)_n$ domains. On the other hand, in the case of VO_x catalysts, a gradual shift in the symmetric stretching of the vanadyl (V=O) Raman band with increasing CeO_2 content was observed that points at the gradual anchoring of the surface vanadia

species on both TiO_2 and CeO_2 thus highlighting the possible existence of the amorphous VO_x to be located at the interface of the two mixed oxides. The catalytic behavior of Mo and V were distinct. As the ceria content in the support increased, MoO_x catalysts promoted the ODHE via Mars van Krevelen mechanism while VO_x catalysts appeared to favor ethane direct dehydrogenation. Investigation of structure-function relationships via in-situ Raman spectroscopic efforts revealed that adding ceria not only changed the redox properties of the support but also improved those of the deposited metal oxide. We also show that upon incorporation of ceria into the support, CO_2 directly participates in the reoxidation of the dispersed MoO_x species during catalysis. This effect was distinct from the reaction of CO_2 in the reverse water gas shift reaction. Operando Raman spectra revealed that the presence of CO_2 enhances the stability of the bridging Mo–O–Mo bond of polymeric molybdena domains, which is proposed to affect the relative contribution of oxidative versus non-oxidative pathways in ethane dehydrogenation.

1 INTRODUCTION

Catalytic oxidative dehydrogenation (ODH) of low molecular weight alkanes has been increasingly gaining interest as an alternative to the direct thermal dehydrogenation route[1,2] towards the production of the corresponding olefins. Among olefins, ethylene (C_2H_4) comprises a valuable intermediate in petrochemical industry. In light of the recent shale gas revolution[3], abundant ethane (C_2H_6) reserves serve as the steppingstone and strong incentive for academic and industrial communities to advance and evolve novel research strategies for the targeted production of ethylene. The requirements of modern catalytic processes for ODH of ethane demand a paradigm shift where rational design of materials directly aims to guarantee high selectivity to olefins by improving redox properties, hampering consecutive olefin overoxidation, limiting coke formation, or enhancing in-situ coke removal pathways[4]. Utilizing carbon dioxide (CO_2) as an

oxidant in ODH has been recognized in recent years as a promising alternative approach that offers an attractive solution to severe total oxidation of ethylene resulting in higher selectivity to desired products[5]. Since CO_2 is the greatest contributor to global climate change, identification of selective reaction pathways in ODH involving CO_2 can potentially improve the performance of this important reaction while simultaneously reducing its carbon footprint.

It is generally accepted that the alkane ODH reaction over several families of supported metal oxide catalysts is strongly dependent on the intrinsic acid-base properties and/or redox properties of the catalysts used, as well as the interaction between active sites and the support materials[6–10]. These effects have spurred research focusing on the rational engineering of catalyst supports either via doping or mixing different metal oxides with the goal of tuning the aforementioned properties in a desirable manner[6,7,11,12]. Besides support effects, post-modification of these supports by depositing secondary active sites in order to improve either the selectivity to olefins or to enhance material stability in conventional ODH with O_2 has also been carried out[6,13]. However, the aforementioned effects are not clear in the case of ODH with CO_2 if one takes into account the complex reaction network that can occur simultaneously[14]. In addition, the reaction mechanism and role of CO_2 as an oxidizing agent in ODH still remains elusive. The majority of studies revealed that the oxygen assisted ODH over many classes of supported metal oxides occurs via a Mars van Krevelen (MvK)[13,15,16] mechanism with the participation of lattice oxygen (Eqs. 1-2) .

$$C_2H_6 + M\text{–}O \rightarrow C_2H_4 + H_2O + M\text{–}\nu_o \quad (1)$$

$$M\text{–}\nu_o + \frac{1}{2}O_2 \rightarrow M\text{–}O \quad (2)$$

On the other hand, many reports concerning CO_2 assisted ODH have demonstrated the combination of direct dehydrogenation (DH) (Eq. 3) and reverse water shift (RWGS) (Eq. 4)[12,14,17–19] as the primary reaction pathways.

$$C_2H_6 \rightarrow C_2H_4 + H_2 \text{ (3)}$$

$$CO_2 + H_2 \leftrightarrow CO + H_2O \text{ (4)}$$

Additionally, in-situ coke removal via reverse Boudouard[17,19,20] mechanism (Eq. 5) and catalyst re-oxidation by CO_2 splitting[17,21] (Eq. 6) have also been proposed to address i) the complex reaction network and ii) the role of CO_2 in promoting catalyst stability.

$$CO_2 + C \rightarrow 2CO \text{ (5)}$$

$$M\text{–}\nu_o + CO_2 \rightarrow M\text{–}O + CO \text{ (6)}$$

However, the dearth of concrete evidence about the different reaction pathways occurring simultaneously in CO_2-assisted ODH over a wide-range of catalyst materials hinders our ability to establish a directional methodology for material improvement at the molecular level.

Among investigated catalysts, dispersed metal oxides such as MoO_x, WO_x, VO_x etc., supported on TiO_2[8,10] have been highlighted to be catalytically active materials for C-H activation, which is the rate limiting step in ODH of ethane. In addition, the physicochemical properties of TiO_2 can be modified via the incorporation of CeO_2[22–24]. It is also noteworthy to mention that mixed CeO_2-TiO_2 supports have shown improved reactivity in other selective oxidation reactions such as the oxidation of dicloroethane[25]. In this work, we study the performance of ODH of ethane over two classes of well-known ODH-active metal oxides, MoO_x and VO_x, deposited on TiO_2 and mixed CeO_2-TiO_2 supports. This study focuses on unraveling the effect of various active sites (Mo, V) as well as nature of the composition of mixed CeO_2-TiO_2 support on the CO_2-assisted ODH of ethane. Efforts are made to understand possible competing ethane conversion pathways and how CO_2 affects the relative performance of different catalysts. In-situ and Operando Raman spectroscopy is utilized in an attempt to develop novel structure-reactivity correlations for the CO_2 assisted ODH of ethane.

2 EXPERIMENTAL SECTION

2.1 Catalyst preparation

$Ce(NO_3)_3.6H_2O$ (99.99%), $Ti(OCH_2CH_2CH_2CH_3)_4$ (97%), TiO_2 (99.9% Degussa P25), $(NH_4)_6Mo_7O_{24}.4H_2O$ (99.98%), NH_3VO_3 (99%) was purchased from Evonik. Mixed CeO_2-TiO_2 was synthesized by following a sol-gel method as reported elshewhere[25,26]. In sol-gel synthesis, typically, solution A was prepared by vigorously stirring a mixture of 10 g $Ti(OC_4H_9)_4$, 3 mL of CH_3COOH and 40 mL of C_2H_5OH. The pH of the solution was then adjusted to 2-3 via dropwise addition of HNO_3. For solution B, an amount of $Ce(NO_3)_3$ was dissolved in 4 mL of deionized H_2O and 20 mL of C_2H_5OH. Solution B was then added dropwise into solution A under vigorous stirring to form a transparent, homogeneous solution. The resulting solution was aged at room temperature for 1 hr and then was heated up to 70 °C where was kept for 2 hrs in order to form a gel. The concentration of solution B was varied to modify the Ce content of the resultant material. The gel was dried at 70 °C for 72 hrs and the remaining solid underwent calcination at 600 °C in the presence of 100ml/min air for 4 hrs with a ramp rate of 2 °C/min. The synthesized CeO_2-TiO_2 mixtures were labeled as xCeTi, where x was formulated as:

$$x = \frac{n_{\mathrm{Ce}}}{n_{\mathrm{Ti}}} \times 100\%$$

Molybdenum oxide and vanadium oxide were deposited on P25 and mixed CeO_2-TiO_2 supports by wet impregnation. A calculated amount of $(NH_4)_6Mo_7O_{24}.4H_2O$ or NH_4VO_3 that leads to a final atomic density equal to 5Mo or 5V atom/nm were dissolved in 40 mL of deionized H_2O to form a transparent solution. 1 g of the prepared oxide support was then added into the solution. This slurry mixture was then dried in a rotary evaporator at 40 °C under reduced pressure before being calcined at 600 °C for 4 hrs. The final catalysts were labeled as 5Mo/xCeTi or 5V/xCeTi.

2.2 Characterization techniques

Crystallinity and phase composition of synthesized CeO_2-TiO_2 samples were analyzed by using X-Ray diffraction measurements (XRD). The analysis was carried out with a PANalytical Philips X'Pert X-Ray diffractometer equipped with a Cu-Kα source at 40 kV and 40 mA and angular incidence 2θ between 20° and 90° with 0.05° step and 2.0 s per step. Silicon was used as an external standard reference to determine any possible peak shift.

The specific surface area of the prepared oxide support was estimated through the Brunauer–Emmett–Teller (BET) method using a Quantachrome Autosorb-1 instrument. The BET measurements were carried out at cryogenic condition after degassing samples at 150 °C for 3 h.

Absorbance properties of purchased P25 and prepared CeO_2-TiO_2 were characterized using UV-vis spectroscopy. Diffuse-reflectance UV-visible spectroscopy was carried out in a Thermo Scientific Evolution 3000 spectrophotometer equipped with a Harrick Scientific Praying Mantis diffuse reflectance accessory. Spectra were scanned between 190 nm and 1100 nm in intervals of either 0.5 nm or 2.0 nm. The absolute reflectance standard was collected using a Spectralon® disk.

Raman spectroscopy studies were carried out using a HORIBA LabRAM HR Evolution high spatial and spectral resolution spectrometer. The incident beam (532 nm, 80 mW) was directed on the samples and focused by a 50x long-working distance objective. Collection of the scattered light was achieved with an air-cooled (−75 °C) open electrode 1024 × 256 pixels CCD. The acquisition time and the total number of accumulations were varied within the 5-20 sec and 10-60 ranges respectively. For the in-situ Raman measurements, the laser line was directed into a reaction cell (Harrick Scientific Products Inc.) and relevant reaction mixture flow was provided via mass flow controllers (Alicat Scientific).

2.3 Catalytic studies

The catalytic performance of all synthesized materials was evaluated with a continuous gas flow system through a quartz tube reactor (4 mm ID). Typically, 200 mg catalyst was diluted with 800 mg quartz sand before being loaded into the reactor. The reactor was then heated up to 600 °C in an air flow to ensure a fully oxidized state. The reactor was then flushed with a 50 mL min^{-1} flow containing pure nitrogen in 10 minutes to ensure that no O_2 was remained in the gas lines that could affect initial time-on-stream data. A mixture of reactants, containing 5% C_2H_6, 5% CO_2, and 90% N_2, was then mixed and stabilized with by-pass before being fed into the reactor. Product analysis was performed via an in-line microGC (Agilent 490) equipped with MS5A column (CH_4, CO and H_2) and PoraPlot Q column (CO_2, C_2H_4, C_2H_6, C_3H_6, C_3H_8). Conversion of C_2H_6, selectivity to C_2H_4, and yield of C_2H_4 were calculated respectively as follows:

$$X_{C_2H_6} = \frac{F_{C_2H_6,in} - F_{C_2H_6,out}}{F_{C_2H_6,in}} \times 100\%$$

$$S_{C_2H_4} = \frac{F_{C_2H_4,out}}{F_{C_2H_6,in} - F_{C_2H_6,out}} \times 100\%$$

$$Y_{C_2H_4} = X_{C_2H_6} \times S_{C_2H_4}$$

3 RESULTS AND DISCUSSION

3.1 Structural implications of surface species via in-situ Raman spectroscopy

The prepared CeO_2-TiO_2 supports where characterized via BET, Raman and UV-vis spectroscopies as well as XRD in an effort to identify the basic structural properties of pure and mixed oxides, before impregnation with the active phase (Mo or V); relevant results are shown in Table S1 and Figure S1. The BET surface area analysis of xCeTi samples showed that at low CeO_2 content, a negligible difference was observed as compared to pure titania (P25) while at higher CeO_2 content an increase was observed. Even though XRD and Raman characterization techniques highlight anatase as the main phase present, the visible light absorbance measured in UV-Vis

spectroscopy revealed the presence of a second oxide. A closer look of the Raman and XRD results underscore that there is a gradual decrease in the crystallinity of the anatase phase in the support materials which is also responsible for the increased surface area upon increasing CeO_2. These observation are in very good agreement with reports concerning the same oxide mixture in literature[22,26–28].

Mo and V loading were selected to be identical in the atomic density of the active species, i.e. 5Mo nm^{-2} and 5V nm^{-2}. This value was chosen in order to ensure that monolayer coverage was not exceeded. Raman spectroscopic studies of dispersed molybdena species on common oxide supports and different atomic density loadings have indicated that the MoO_x saturation capacity is around 5-6 atom/nm^2. There is a wealth of information from in-situ spectroscopic studies of supported metal oxides highlighting the importance of characterizing those catalysts under dehydrated conditions to simulate the structure of catalysts under reaction conditions. Since strong structural changes occur upon temperature elevation[29,30] (i.e dehydration of surface species as well as dehydroxylation of the support[31–33]) Raman spectra of deposited molybdenum and vanadium oxides under dehydrated conditions were collected at 600 °C in the presence of air as shown in Figure 1.

The family of supported molybdena on prepared supports (Figure 1a) exhibits a distinct peak at 996cm^{-1}. This peak represents the vibrational stretching mode of molybdenyl double bond (Mo=O)[31,34,35] from $(MoO_x)_n$ dispersed species. In addition, the absence of a strong band at 820cm^{-1} of crystalline MoO_3 is consistent with our design of materials where the formation of three dimensional MoO_3 is prohibited at surface densities below monolayer coverage. In the open literature authors have demonstrated that on TiO_2, as loadings approaches the monolayer coverage, small polymeric Mo species can be formed; an associated shift of the Mo=O stretching mode of

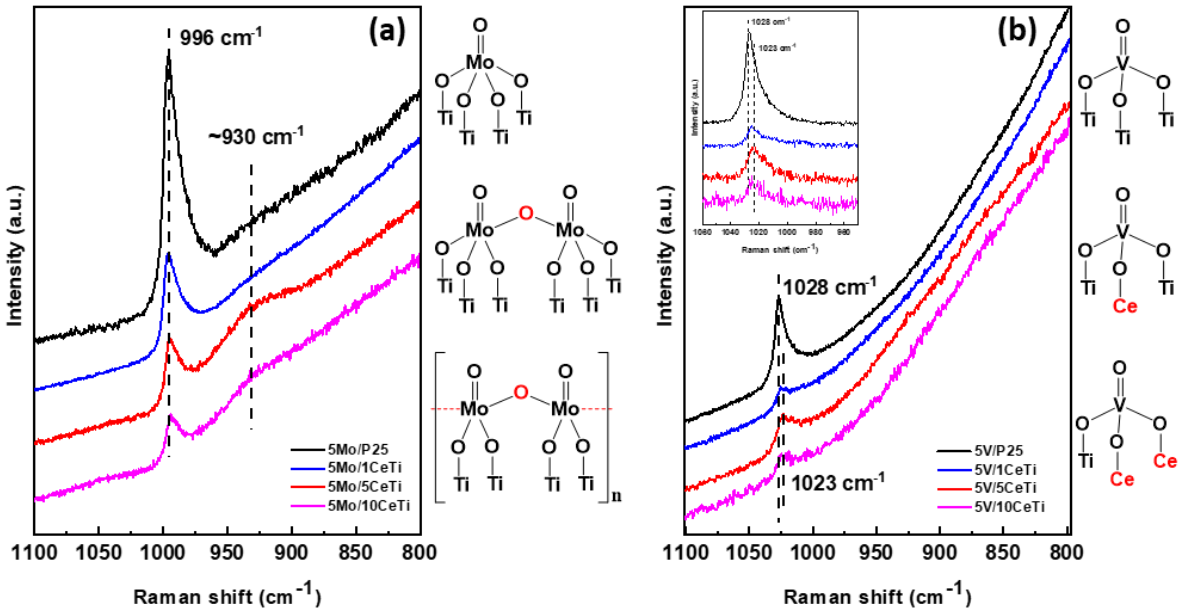

Figure 1: In-situ Raman spectra of (a) Mo and (b) V catalysts supported on different oxides under dehydrated conditions. The inset of Figure 1b shows the Raman spectra of V catalysts subtracted with the spectral contribution of the pure supports. (T=600 °C under 50cc/min of air flow. Acquisition time: 10-60 sec, Number of accumulations: 5-10).

terminal oxygen to higher wavenumbers has been suggested[32,36]. In addition, supported molybdena have been reported to be tuned during synthesis by adjusting the pH of the precursor to achieve different proportions of monomeric or polymeric structures at fixed Mo loadings[29]. As more polymeric domains were formed, the band signifying mono-oxo molybdena shifted from 992 cm^{-1} to 995 cm^{-1} which is consistent with the results shown in Figure 1a. Interestingly, a broad band at ~930 cm^{-1}, which was, however, insignificant in 5Mo/P25 and 5Mo/1CeTi, appeared to be strong in 5Mo/5CeTi and 5Mo/10CeTi catalysts. This band has been assigned in various characterization studies[29,31,33–35,37–45], with a general consensus, to the Mo–O–Mo functionalities of larger $(MoO_x)_n$ polymeric domains of the dispersed phase. In addition, upon CeO_2 increase, the peak intensity at 996 cm^{-1} appears to decrease significantly with a monotonic increase in the 930cm^{-1} band which is associated with the Mo–O–Mo units. Based on the Raman spectroscopic behavior in conjunction with XRD results discussed above we suggest that dispersed amorphous MoO_x units preferentially anchor on the crystalline domains of TiO_2. When ceria is dispersed into

the support, the crystallite size and overall crystallinity of anatase TiO_2 shrinks, thus leaving less free anatase surface area for molybdena to be anchored which in turn promotes the formation of polymeric species. The possibility that changes in crystallinity upon CeO_2 addition might also affect the dominant exposed facets thus promoting the formation of larger polymeric species with different apparent degrees of polymerization cannot be excluded. However, further studies via advanced microscopy characterization can provide invaluable insights into this research aspect.

To shed some light into the molecular structure of vanadium catalysts, their Raman spectra under dehydration conditions are shown in Figure 1b. The 5V/P25 catalyst exhibited a well-defined band at 1028 cm^{-1} which is assigned to monomeric mono-oxo structure of vanadium oxide[35]. The intensity of the terminal vanadyl oxygen band dropped significantly when more ceria was incorporated into the support, similar to the Mo catalysts. Although the position of the terminal Mo=O stretching band was unchanged irrespective of CeO_2 content in support phase, the band position of the relevant V=O band gradually red shifted to 1020-1023 cm^{-1} as more CeO_2 was added due to electron-withdrawing effects of the support via M–O–V bonds[35,46]. On pure CeO_2, the monomeric oxo-structural VO_x species were reported[35] to exhibit a band at 1023 cm^{-1}. It has been recognized[7,47] that in mixed supports with high Ce content, VO_x species prefer to anchor on CeO_2 with the unavoidable consequence of forming stable mixed phase cerium vanadate ($CeVO_4$) at high temperatures which in turn negatively affects the catalytic reactivity of those materials. The Raman spectroscopic "fingerprints" of $CeVO_4$ were not detected in the present study up to 600 °C. The sol-gel synthesis method followed in this study guaranteed that small, well-dispersed CeO_2 crystallite domains are formed, which in turn can prevent the formation of mixed $CeVO_4$ crystals. This could arise from the deposition of VO_x species at the interfacial region of CeO_2 and TiO_2 where some M–O–V anchoring bonds formed to the TiO_2 phase and some to the CeO_2.

The results shown above reveal distinct patterns in the molecular structure of the synthesized materials where polymeric functionalities are promoted on Mo catalysts upon ceria addition while only monomeric VO_x units dominate the interface of CeO_2–TiO_2. With the intention to provide structure-reactivity relationships via molecular level understanding, the next sections focus on evaluating the catalytic performance of all catalysts synthesized as well as further elucidating possible structural implications on chemical reactivity

3.2 Catalytic performance of supported Mo and V on P25 and mixed CeO_2-TiO_2

Preceding any discussion of the catalytic behavior of our supported catalysts, it is important to briefly discuss the catalytic reactivity of the bare supports, summarized in Figure S2 of the supporting information. P25 exhibited 11.5% ethane conversion with an initial ethylene selectivity of 82%. The addition of a small amount CeO_2 in the mixed 1CeTi support did not cause any significant changes as compared to P25. Upon further increase of CeO_2 content in the mixed support, both ethane conversion and ethylene selectivity decreased. This decrease is correlated with the decrease in TiO_2 crystallinity observed by XRD and Raman with increased ceria content. Ceria may also be blocking some ethane dehydrogenation sites on the TiO_2 surface while simultaneously altering the crystallinity, thus fewer active sites are present. It should be noted that other studies have shown an increase in reducibility when small ceria particles are dispersed in a mixed oxide system[48], and especially in TiO_2 based systems[49]. Furthermore, when ceria was used as a modifier and oxygen buffer, alkane overoxidation was enhanced[50]. As the loss of ethylene selectivity was due to overoxidation to CO and CO_2, the enhanced oxygen storage and oxygen mobility in high ceria loadings can explain the drop in selectivity.

The addition of dispersed MoO_x and VO_x on the surface of all catalyst supports was evaluated and relevant results regarding their catalytic performance are depicted in Figure 2. In the case of P25 (**Figure 2**a), the addition of molybdenum and vanadium oxides enhanced the initial ethane

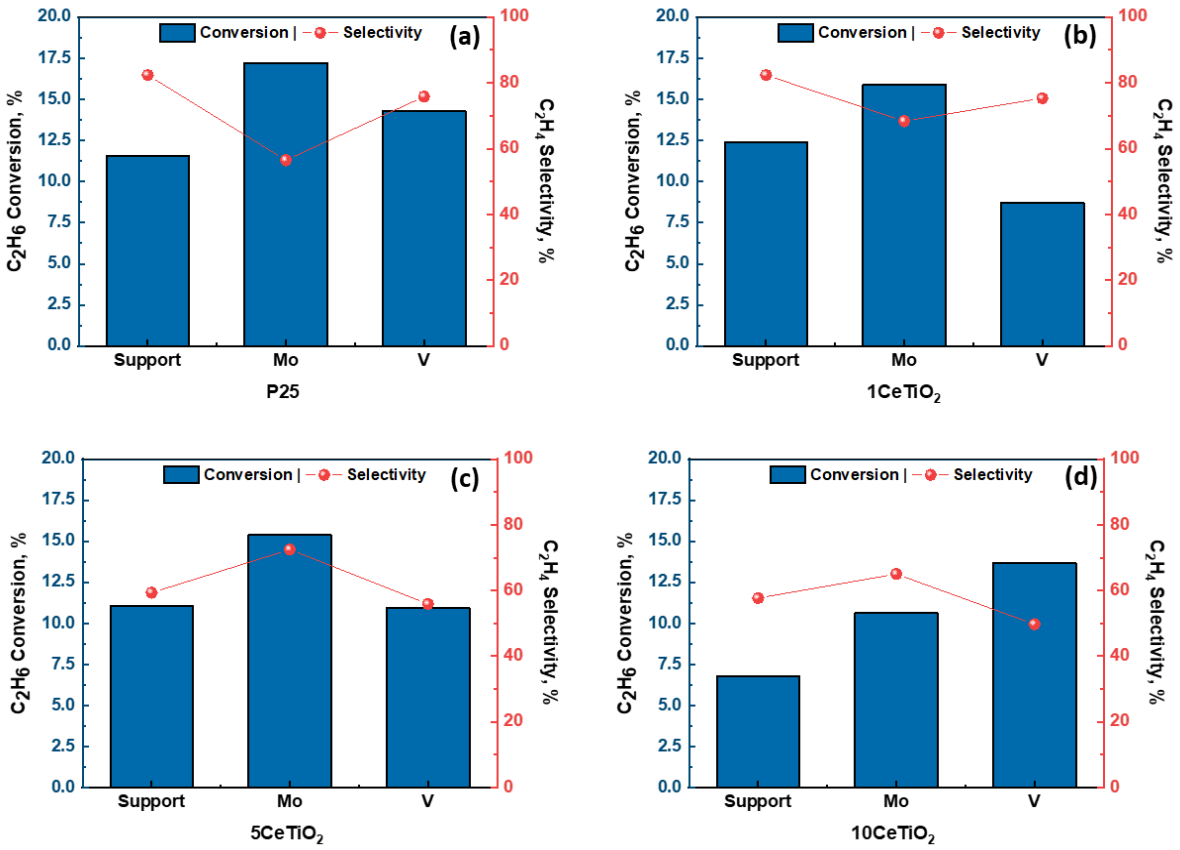

Figure 2: Initial conversion ethane and selectivity to ethylene over molybdenum and vanadium oxide on different supports at 600 °C, under a 20 mL flow containing 5% C_2H_6, 5% CO_2 and 90% N_2.

conversion as compared to the bare supports with the Mo catalysts showing the larger effect. This underscores that the presence of MoO_x reactive sites on supports contributes to the excess ethane conversion. In conventional ODH with O_2, it was reported that with greater Lewis acidity at cationic sites, C-H activation for alkanes to alkenes as well as the non-selective activation of the π bond (usually leads to combustion) was more facile [16]. Since the Lewis acidity of Mo^{6+} is stronger than that of V^{5+}, it is expected that supported MoO_x species can lead to higher ethane conversion but with relatively lower selectivity to ethylene than supported VO_x. Our results are consistent with this hypothesis and show almost 20% less ethylene selectivity in Mo/P25 than V/P25. As these trends from conventional ODH are preserved in the CO_2-asssited ethane ODH in the present work, a similar reaction mechanism between the two systems is implied.

Upon addition of Mo and V species on the surface of CeO_2-TiO_2 supports the catalytic performance data revealed different trends. As seen in Figure 2, deposition of molybdenum oxide on all supports significantly promoted ethane conversion as compared to the bare supports. A maximum selectivity to ethylene of 72% was measured for the 5Mo/5CeTi catalyst. In contrast, the effect of V addition varied with Ce content. The low Ce support 1CeTi decreased the conversion of ethane significantly with almost no change in ethylene selectivity as compared to the bare 1CeTi support. Increasing the CeO_2 content of the support tended to increase ethane conversion and decrease the olefin selectivity. Although dispersed VO_x and MoO_x were commonly referred to as having similar active sites due to the similar oxo-structure of the deposited phases[15,16,51], the vanadium-based catalysts follow a quite different catalytic behavior than the molybdenum-based catalysts.

This divergence in catalytic behavior between Mo and V catalysts on mixed CeO_2-TiO_2 is related to their distinctive structures on these supports. Previous reports on conventional ODH with O_2 have associated the terminal molybdenyl oxygen (Mo=O) with combustion pathways of alkanes and olefins, while anchoring and bridging oxygens have been associated with selective conversion of alkanes to alkenes[8,10,13]. In the present system, the Raman spectra in Figure 1 revealed that the intensity of the Mo-O-Mo stretches increased with increasing Ce content of the support, reinforcing the same trend with increasing selectivity suggested in previous work. In contrast, ethylene selectivity of V catalysts decreased with increasing Ce content in the support. Ethylene selectivity over V catalysts appears to follow a behavior similar to that observed on the bare supports, supporting the hypothesis regarding proximity of V species and Ce sites on the surface. Next, we focus our efforts on investigating possible structure-reactivity relationships by coupling catalytic measurements with in-situ Raman spectroscopy.

3.3 Effect of support and active sites on C_2H_6 conversion pathways

Due the existence of multiple proposed dehydrogenation mechanisms on metal oxide catalysts, the influence of each catalyst active site on the flux through difference reaction pathways in CO_2-assisted ODH is complex. Oxidative dehydrogenation pathways lead to water as a product (e.g. Reaction 1), while pure dehydrogenation leads to H_2 as a product (Reaction 3) [7,14,19,21,52]. However, the amount of hydrogen in the reactor effluent is also influenced by the extent of reverse water-gas shift due to the presence of CO_2 in the feed (Reaction 4). Therefore, the relative amounts of different species in the effluent can offer clues for the dominant pathways in play over a given catalyst, or during specific reaction conditions.

An added complication is that the oxidation state of the catalyst and/or support may vary as the reaction proceeds. For this reason, the initial reactivity, when the catalyst is still fully oxidized, can give insight into the intrinsic competition between dehydrogenation (DH) and ODH of ethane at the same active sites. At sufficiently low CO_2 conversion (<5%) the extent of H_2 consumption via RWGS is limited, so the ratio of hydrogen to ethylene in the reactor effluent can serve as an indicator for the relative contribution of DH and ODH of ethane reaction pathways. The CO_2 conversion was very low within the first hour of time-on-stream, so initial rate data were suitable for this comparison. The ratio $\boldsymbol{\gamma}$, is defined at the reactor outlet as:

$$\boldsymbol{\gamma} = \frac{\text{molar flow rate of } H_2}{\text{molar flow rate of } C_2H_4}$$

In the case where direct dehydrogenation (Reaction 3) is the sole contributor to olefin formation, this ratio is expected to have a value equal to one. If one allows for additional side reactions such as C-C cracking or combustion of the olefin, the value may even exceed one. In contrast, the MvK mechanism for ODHE (Reactions 1-2) alone would result in a ratio equal to zero.

Figure 3 depicts the effect of CeO_2 addition in the support material on the **γ** ratio at early reaction times. Comparing the performance of the bare supports, it is observed that **γ** ratio slightly increases with higher ceria content, indicating higher direct dehydrogenation activity. Interestingly, in the case of Mo catalysts, the initial **γ** ratio of Mo/P25 was approximately 1, and therefore ethane conversion occurred mainly through direct dehydrogenation. However, when molybdena was deposited on mixed CeO_2-TiO_2, the initial **γ** ratio dropped significantly to a value of ~0.1 and varied little with CeO_2 content. The dramatic shift indicated very low direct dehydrogenation and implies that all or nearly all of the ethane conversion occurs via oxidative dehydrogenation once CeO_2 is introduced into the support. By contrast, vanadium catalysts showed a very similar trend in **γ** ratio to the bare supports, only with slightly higher **γ** ratios. Unlike Mo, which performed less direct dehydrogenation in the presence of ceria, V catalysts actually became more competent at direct dehydrogenation and less competent at oxidative dehydrogenation.

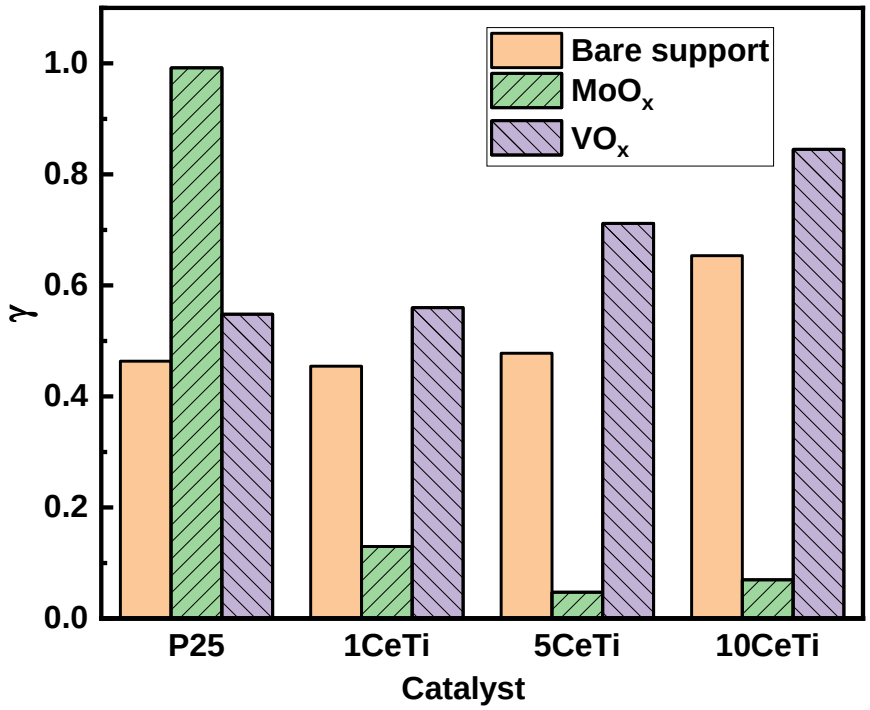

Figure 3: Initial ratio of produced H_2 to produced C_2H_4 over 5Mo/xCeTi and 5V/xCeTi at 600°C under a flow of 20 mL/min containing 5% C_2H_6, 5% CO_2 and 90%N_2

The difference between Mo and V catalysts was further explored by investigating how reaction temperature affects the **γ** ratio. 5Mo/5CeTi and 5V/10CeTi were selected to represent the extreme cases where either direct dehydrogenation or oxidative dehydrogenation were dominant at early reaction times. Figure S6 plots the initial **γ** ratio as a function of temperature for these two materials. 500 °C is a low enough temperature that the endothermic direct dehydrogenation reaction is thermodynamically unfavorable, so the exothermic oxidative dehydrogenation dominates over both catalysts, leading to low **γ** ratios. Although even at this low temperature the V catalyst produces more hydrogen, and therefore direct dehydrogenation, the Mo catalyst produced almost no hydrogen at all. As temperature was increased, the initial **γ** ratio of both catalytic systems increased, with the ratio of Mo catalyst always significantly lower than that of V catalysts. However, the **γ** ratio over Mo was still low at ~0.3 even at 650 °C, while the ratio over V increased significantly at 600 °C as the temperature was high enough to promote the endothermic reaction, and reached 0.85 at 650 °C, highlighting the large difference in catalytic behavior of the two catalysts with regard to direct and oxidative dehydrogenation pathways.

C-H bond activation has been shown to occur on lattice oxygen species of supported metal oxides in the Mars-van Krevelen mechanism of oxidative dehydrogenation[44,45]. On the contrary, a metallic interaction is crucial to break C-H bonds in the direct dehydrogenation mechanism over supported metal catalysts[4]. In the present study, initial ethane conversion seems to occur in large part through direct participation of lattice oxygens over Mo, with the natural consequence of rapidly reducing the oxidation state of the active sites as lattice oxygen is removed. The time-on-stream dependence of the **γ** ratio presented in Figure S7 shows that at long reaction times, the value of the **γ** ratio converged for all Mo catalysts indicating that due to deep reduction similar MoO_{x-n} surface species across samples may exist. On the other hand, distinct values were observed

for V catalysts. This behavior could be associated with the fact that V catalysts may preserve their initial reactivity and selectivity (Figure S3) throughout the course of the experiments which is also consistent with the preceding discussion on promoting mainly the direct dehydrogenation pathway.

Although CO_2 is utilized as a mild oxidizing agent, whether it can effectively replenish the lattice oxygen lost in the MvK mechanism, especially for the Mo catalysts, remained an open question. Dynamic Raman spectroscopy was used to investigate the effect of CeO_2 in the support on the redox properties of the active site. The catalysts were reduced in 0.5 % H_2 at 600 °C, and the results of in-situ Raman measurements are shown in Figure 4a-d. Although the terminal Mo=O oxygen from molybdena is hypothesized to be associated with non-selective combustion of ethane, changes in the intensity of this peak could still be utilized as an indicator of the overall material oxidation state. When exposed to hydrogen, the intensity of the 995 cm^{-1} peak of all materials decreased with time signifying reduction. From Figure 4d, it is evident that the reduction of the Mo=O peak over P25 is much slower than over 1CeTi, and over 5CeTi the rate of reduction was faster still. The spectroscopic signature of the Mo=O peak in the 10CeTi sample could not be recorded by in-situ Raman due to its very weak intensity (discussed above) in conjunction with the rapid rate of reduction of this catalyst. This enhancement highlights a significant improvement

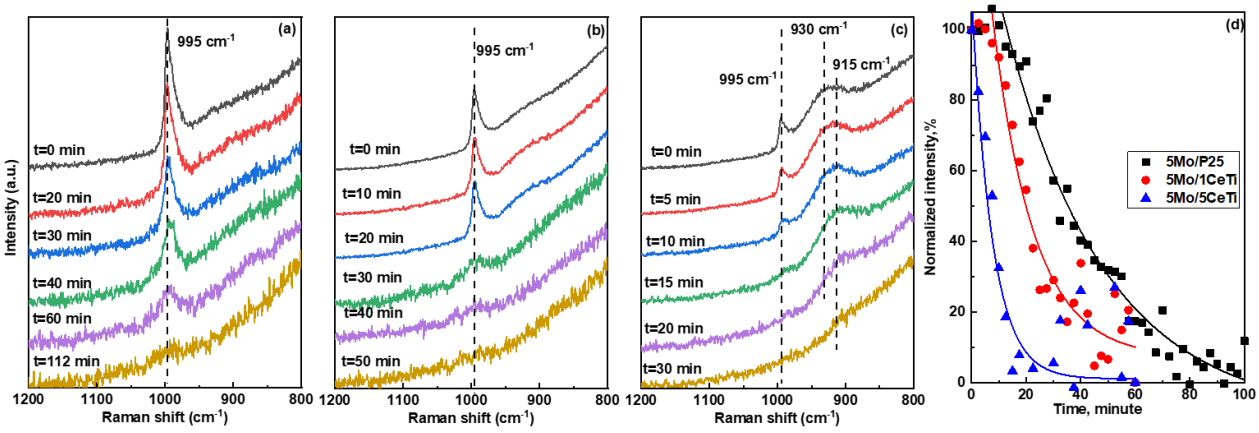

Figure 4: In-situ Raman spectra of reduction over (a) 5Mo/P25, (b) 5Mo/1CeTi, (c) 5Mo/5CeTi at 600°C under a 50mL/min flow containing 0.5 % H_2, and 99.5 % N_2. (d) Normalized intensity change of Mo=O peak

in reducibility of supported molybdena on mixed ceria-titania as opposed to on pure P25. Our results are consistent with H_2 TPR studies showing that ceria dispersed in titania improves the reducibility of mixed oxides[25,27]. The improvement in the redox properties of the support also directly affects the reducibility of the dispersed active phase, which in turn is expected to play a crucial role in ODH via MvK where the removal of hydrogen from ethane and the release of water strongly depends on the reducibility of active sites[4,13,16].

In the case of 5Mo/5CeTi, the spectroscopic Raman signature for lattice oxygen in bridging Mo-O-Mo bonds is clearly identified initially at 930 cm^{-1}. The intrinsic behavior between bridging and terminal oxygens during reaction conditions were investigated by operando Raman spectroscopy (Figure 5) under flow conditions identical to those of the catalytic reaction experiments. Figure 5 illustrates the relative decrease in the peak intensities of both Mo=O and Mo–O–Mo features over time in the presence of ethane/CO_2 mixture in the gas phase. Although the general trend observed was similar to that when exposed to hydrogen (Figure 4c) the overall

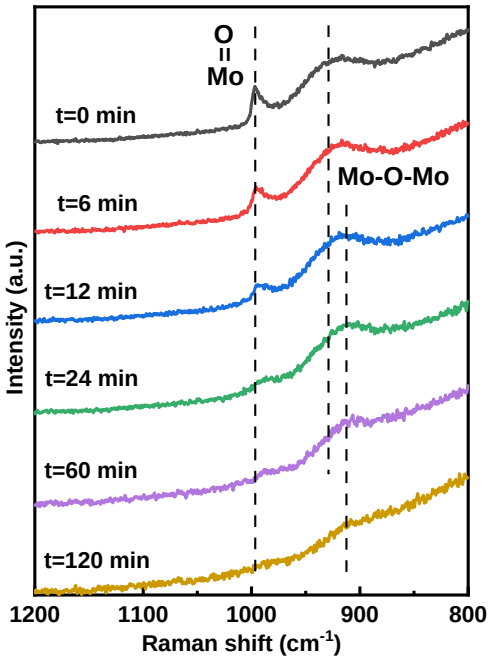

Figure 5: (a) Operando Raman spectra of 5Mo/5CeTi under a 50 mL/min flow containing 2% C_2H_6, 2% CO_2, and 96 % Ar at 600°C. Time on stream γ ratio of (b) Mo catalysts, (c) V catalyst in reaction carried out 600°C, under a 20 mL/min flow containing 5 % C_2H_6, 5 % CO_2, and 90 % N_2

Mo=O as well as Mo-O-Mo reduction was slower when the reducing agent is ethane. Clearly both bridging and terminal oxygen sites are implicated in ethane conversion. A red shift from 930 cm^{-1} to 920 cm^{-1} for the bridging oxygen species was observed over the course of the reaction under hydrogen flow as well as reaction conditions. The peak intensity at 995 cm^{-1} decreased at a higher rate than that of 930 cm^{-1}, indicating sequential loss of terminal and bridging oxygen species. As the population of bridging oxygen species decreased, polymeric domains of molybnena could be expected to divide and form smaller domains. These smaller domains of polymers were less electron withdrawing at each Mo site, causing the red shift of the bridging oxygen peak[53].

Together, the dynamic depletion of lattice oxygen species observed by Raman spectroscopy and the changes in the $\boldsymbol{\gamma}$ ratio with time-on-stream can explain the reactivity trends in supported Mo catalyst (Figure 5). Initially, the catalyst is fully oxidized, and the bridging oxygen atoms serve as active sites for alkane conversion via oxidative dehydrogenation[8]. This would deplete the concentration of the active site rapidly, but is mitigated somewhat by the presence of the terminal oxygen groups. These terminal oxygen atoms migrate to bridging positions, and therefore are depleted first and prolong the ODH activity of the catalyst. CO_2 may reoxidize some sites, but the fast depletion of the terminal oxygen signal indicates that the reoxidation rate must be slower than the oxygen removal rate. Eventually, no terminal oxygen peak remains, and bridging oxygens begin to be depleted, dividing polymeric molybdena islands into smaller domains. The $\boldsymbol{\gamma}$ ratio increases as the oxygen-depleted catalyst begins to perform more direct dehydrogenation. Samples with higher ceria content in the support maintain ODH activity longer due to the higher oxygen mobility in the support.

These trends observed over Mo are absent over V and over bare supports. These catalysts always show higher $\boldsymbol{\gamma}$ ratio and therefore primarily convert ethane via direct dehydrogenation. As little

ODH takes places under the current reaction conditions, changes in oxidation state of these materials do not affect selectivity. On the contrary, in supported VO_x catalysts, some of the anchoring oxygens have been reasoned earlier that could be connected with more Ce atoms instead of Ti atoms (red shift of V=O with increasing CeO_2). Thus, one expects that depending on the initial VO_x mono-oxo configurations (more V-O-Ti or more V-O-Ce), the initial reduced state of V sites of 5V/xCeTi can diverse significantly. These structural implications could explain the different **γ** ratio behavior over the V catalysts both at initial conditions as well as longer time-on-stream.

The interconversion of terminal and bridging oxygen species and the extent to which CO_2 reoxidizes the Mo catalyst was investigated via in-situ Raman spectroscopy, with results shown in Figure 6. 5Mo/5CeTi was reduced under reaction conditions at different CO_2. Figure 6 shows the Raman spectra in the presence of ethane without CO_2 in the feed while in Figure 6b an excess of CO_2 was used. In both cases, the reduction of the terminal M=O bond was rapid and essentially identical. As discussed previously, rapid depletion of the M=O signal and slower depletion of the

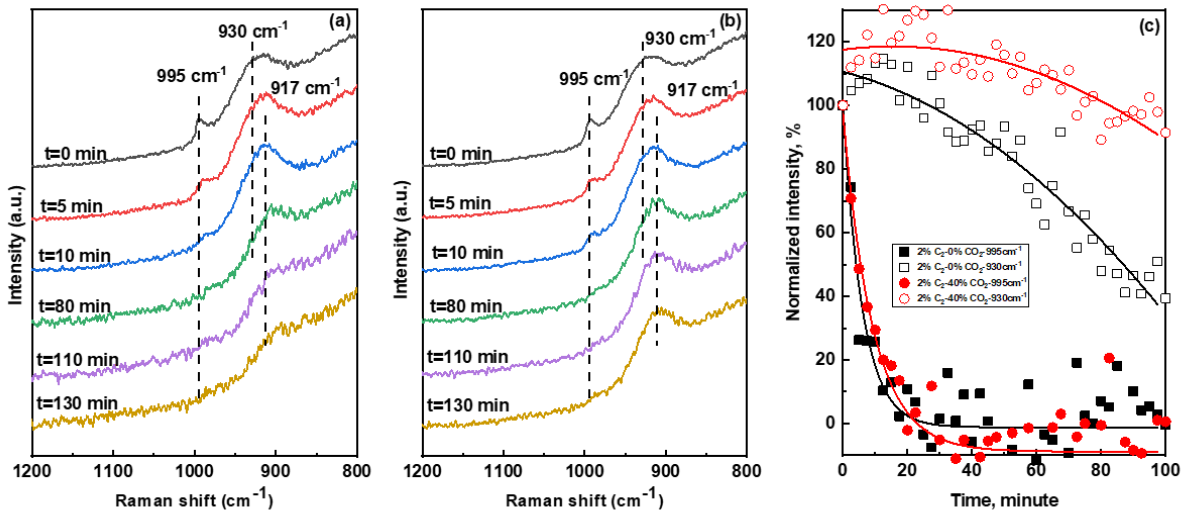

Figure 6: In-situ Raman spectra of 5Mo/5CeTi at 600ºC under a 50mL/min flow containing (a) 2 % C_2H_6, and 98% N_2 (b) 2 % C_2H_6, 40 % CO_2, and 58 % N_2. (c) Change in peak intensity of molybdenyl and bridging bond during in-situ Raman spectroscopy

bridging Mo-O-Mo signal indicates interconversion of oxygen between these two reactive sites. Because the presence of CO_2 did not impact the terminal Mo=O signal depletion rate, it can be inferred that terminal oxygens are more effective at replacing bridging oxygens removed by the reaction, and that CO_2 is ineffective at replenishing terminal oxygens in this system. However, when excess CO_2 was co-fed into the reactor, the bridging oxygen signal of polymeric Mo species was depleted more slowly than in the absence of CO_2. This apparently slow reoxidation of the catalyst may occur by directly adding oxygen to bridging bonds, or by adding oxygen to terminal positions which then rapidly rearrange to bridging positions. It has been also shown previously that during reduction by H_2 of MoO_3/TiO_2 catalysts, the lattice Mo-O-Ti as well as Ti-O-Ti oxygen sites were reduced first. Exposing the catalysts to $^{18}O_2$ led to a tandem reoxidation scheme where the anchoring lattice oxygen sites are replenished first, followed by a surface oxygen spillover to recover Mo=O functionalities[54]. A similar behavior in the present system where CO_2 splits over the lattice oxygen sites with a subsequent migration to the Mo-O-Mo bonds cannot be excluded. However, as the reverse water-gas shift reaction also influences CO_2 conversion, beside possible material reoxidation, the overall role of CO_2 in the reaction is discussed in the following section.

3.4 Effect of support and active sites on CO_2 conversion

The existence of multiple simultaneous reaction pathways, as inferred by the analysis of the **γ** ratio as well as the spectroscopic results above, makes the attempts to unveil the effect of CO_2 on catalytic reactivity more relevant than ever. As shown above, at long time-on-stream during reaction over supported Mo catalysts, the direct dehydrogenation pathway appeared to dominate the overall ethane conversion as opposed to ODH at early reaction times. The time-on-stream data of the **γ** ratio show a rapid change at early reaction times underscoring a shift in reaction pathways for ethane conversion. In order to maintain the initial behavior of Mo catalysts, i.e. ODH via MvK mechanism, surface MoO_x species need to be reoxidized using CO_2. Although it is believed that

RWGS is not the sole reaction path of CO_2 (ethane reforming[52] and reverse Boudouard[19] can be present), it is still unclear whether the dispersed active surface species are able to be reoxidized with CO_2. Considering that the rapid oxygen depletion of surface species (Figure 6) is responsible for the initial catalyst deactivation (Figure S3-4), an effort was made to understand reoxidation of surface species with CO_2.

An in-situ Raman study, whose results are plotted in Figure 7a-c, was conducted over the 5Mo/xCeTi where the catalyst was initially reduced with hydrogen and subsequently reoxidized

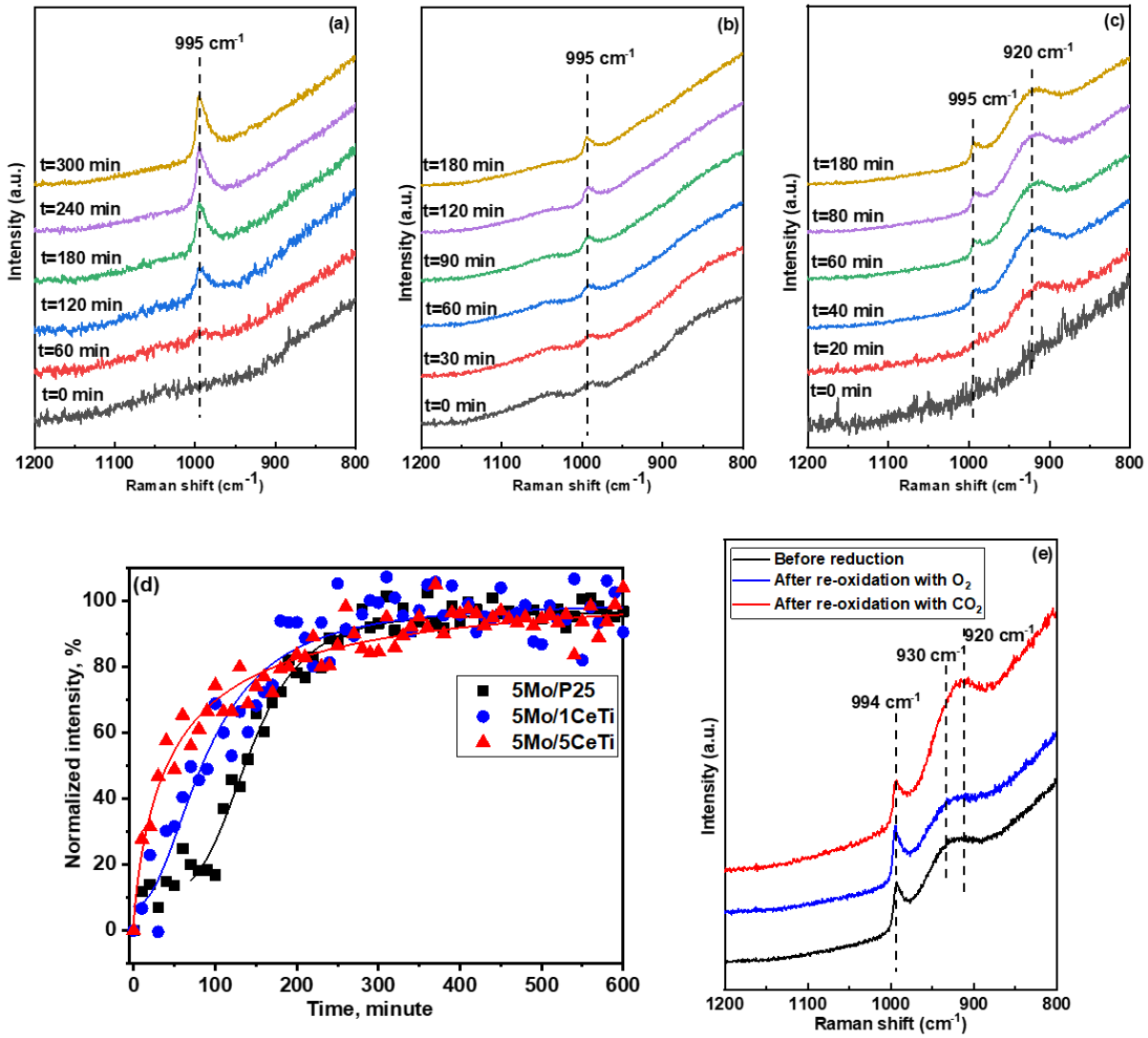

Figure 7: In-situ reoxidation at 600 °C under a 50 mL/min flow containing 60 % CO_2 and 40 % N_2 over (a) 5Mo/P25, (b) 5Mo/1CeTi, (c) 5Mo/5CeTi. (d) Raman spectra of 5Mo/5CeTi before reduction and after re-oxidation with O_2 and CO_2

with CO_2. After reduction, neither the peaks that correspond to the terminal (Mo=O) nor bridging (Mo–O–Mo) were visible in the Raman spectra. In the presence of CO_2, both of these peaks gradually increased with time, indicating that CO_2 was indeed reoxidizing reduced surface sites. However, their intrinsic rates of reoxidation vary significantly with catalyst support. Specifically, the rate of reoxidation is faster with higher ceria content in the support, as illustrated in the spectral analysis of Figure 7d. Despite this enhancement in the oxidation rate, the rate of reduction of Mo catalysts (Figure 4d) was still an order of magnitude faster than reoxidation by CO_2. In addition, Figure 7e shows Raman spectra of 5Mo/5CeTi catalysts reoxidized with either O_2 or CO_2 compared to the as-prepared sample prior to reduction After reoxidation with O_2, 5Mo/5CeTi showed identical spectral features to that of the fully oxidized material, in particular in recovering the Mo–O–Mo peak at 930 cm^{-1}. However, in the case of CO_2 assisted reoxidation, the recovered Mo–O–Mo peak exhibits a red shift to 920 cm^{-1}. This red shift indicates that the CO_2 treatment was not able to recover all the polymeric Mo domains, leaving smaller Mo oligomers on the catalyst surface. The impact of this incomplete reoxidation by CO_2 is shown in Figure S7, where catalysts were regenerated by O_2 and by CO_2. This study showed that the catalysts could regain full activity with negligible difference after being regenerated with O_2, while regeneration with CO_2 led to only partial recovery of the original activity.

This mismatch in redox rates between fast reduction of Mo centers during reaction and slow, incomplete reoxidation by CO_2 gradually depleted the surface of reactive oxygen species as a function of time on stream. The ability of Ce content to influence the reoxidation rate indicates that these rates are material properties that can be tuned, and opens up avenues for future research into engineered materials with compatible redox rates, leading to stable ethylene production at low reaction temperatures with ODHE as the dominant pathway.

4 CONCLUSIONS

Supported surface molybdena and vanadia on pure P25 and mixed CeO_2-TiO_2, prepared by sol-gel method, were catalytically evaluated for the CO_2-assisted ODH of ethane Based on Raman characterization, it was shown that surface Mo species tend to anchor on the crystalline domains of anatase. On the other hand, vanadia was located in the proximity of Ce, resulting in VO_x anchoring to more Ce atoms. With increased ceria content in the support, initially, Mo catalysts produced ethylene via ODH of ethane though a MvK mechanism, while supported V catalysts showed reactivity similar to bare supports and primarily catalyzed the DH pathway for ethane conversion. At longer time-on-stream, a shift in ethane conversion pathways was observed that is associated with the depletion of reactive MoO_x sites.

The incorporation of ceria into the mixed oxide support improved the redox properties of catalyst system. The bridging Mo–O–Mo bond appeared to be more robust in the presence of ethane and CO_2 while the Mo=O was rapidly lost due to reduction under reaction conditions, irrespective of whether CO_2 was present. CO_2 was a competent oxidant. In the absence of a reducing agent, CO_2 was able to recover both the terminal and bridging molybdenum-oxygen signals in Raman (as seen also when oxidizing with O_2), but the recovery of Mo–O–Mo was at a much lesser extent during reaction conditions.

Author Contributions

The manuscript was written through contributions of all authors. All authors have given approval to the final version of the manuscript.

Funding Sources

This work was conducted with funding from the RAPID manufacturing institute, supported by the Department of Energy (DOE) Advanced Manufacturing Office (AMO), award numbers DE-

EE0007888. The current RAPID project was also made possible in part by funding provided by

Rutgers, The State University of New Jersey.

ACKNOWLEDGMENT

The authors would like to thank Prof. Alex V. Neimark for helping with the BET measurements.

REFERENCES

(1) Mimura, N.; Takahara, I.; Inaba, M.; Okamoto, M.; Murata, K. High-Performance Cr/H-ZSM-5 Catalysts for Oxidative Dehydrogenation of Ethane to Ethylene with CO2 as an Oxidant. *Catal. Commun.* **2002**, *3* (6), 257–262. https://doi.org/10.1016/S1566-7367(02)00117-6.

(2) Ren, T.; Patel, M.; Blok, K. Olefins from Conventional and Heavy Feedstocks: Energy Use in Steam Cracking and Alternative Processes. *Energy* **2006**, *31* (4), 425–451. https://doi.org/https://doi.org/10.1016/j.energy.2005.04.001.

(3) Bruijnincx, P. C. A.; Weckhuysen, B. M. Shale Gas Revolution: An Opportunity for the Production of Biobased Chemicals? *Angew. Chemie Int. Ed.* **2013**, *52* (46), 11980–11987. https://doi.org/10.1002/anie.201305058.

(4) Sattler, J. J. H. B.; Ruiz-Martinez, J.; Santillan-Jimenez, E.; Weckhuysen, B. M. Catalytic Dehydrogenation of Light Alkanes on Metals and Metal Oxides. *Chem. Rev.* **2014**, *114* (20), 10613–10653. https://doi.org/10.1021/cr5002436.

(5) Solymosi, F.; Oszkó, A.; Bánsági, T.; Tolmacsov, P. Adsorption and Reaction of CO2 on Mo2C Catalyst. *J. Phys. Chem. B* **2002**, *106* (37), 9613–9618. https://doi.org/10.1021/jp0203696.

(6) Bugrova, T. A.; Dutov, V. V; Svetlichnyi, V. A.; Corberán, V. C.; Mamontov, G. V. Oxidative Dehydrogenation of Ethane with CO2 over CrOx Catalysts Supported on Al2O3, ZrO2, CeO2 and CexZr1-XO2. *Catal. Today* **2019**, *333*, 71–80. https://doi.org/https://doi.org/10.1016/j.cattod.2018.04.047.

(7) Raju, G.; Reddy, B. M.; Park, S.-E. CO2 Promoted Oxidative Dehydrogenation of N-Butane over VOx/MO2–ZrO2 (M=Ce or Ti) Catalysts. *J. CO2 Util.* **2014**, *5*, 41–46. https://doi.org/https://doi.org/10.1016/j.jcou.2013.12.003.

(8) Christodoulakis, A.; Machli, M.; Lemonidou, A. A.; Boghosian, S. Molecular Structure and Reactivity of Vanadia-Based Catalysts for Propane Oxidative Dehydrogenation Studied by in Situ Raman Spectroscopy and Catalytic Activity Measurements. *J. Catal.* **2004**, *222* (2), 293–306. https://doi.org/https://doi.org/10.1016/j.jcat.2003.10.007.

(9) Liu, Y.-M.; Feng, W.-L.; Li, T.-C.; He, H.-Y.; Dai, W.-L.; Huang, W.; Cao, Y.; Fan, K.-N. Structure and Catalytic Properties of Vanadium Oxide Supported on Mesocellulous Silica Foams (MCF) for the Oxidative Dehydrogenation of Propane to Propylene. *J. Catal.* **2006**, *239* (1), 125–136. https://doi.org/https://doi.org/10.1016/j.jcat.2005.12.028.

(10) Tsilomelekis, G.; Christodoulakis, A.; Boghosian, S. Support Effects on Structure and Activity of Molybdenum Oxide Catalysts for the Oxidative Dehydrogenation of Ethane. *Catal. Today* **2007**, *127* (1), 139–147. https://doi.org/https://doi.org/10.1016/j.cattod.2007.03.026.

(11) Lei, T.; Cheng, Y.; Miao, C.; Hua, W.; Yue, Y.; Gao, Z. Silica-Doped TiO2 as Support of Gallium Oxide for Dehydrogenation of Ethane with CO2. *Fuel Process. Technol.* **2018**,

177, 246–254. https://doi.org/https://doi.org/10.1016/j.fuproc.2018.04.037.
(12) Guío, M., Prieto, J. Corberán, V. C. Determination of Kinetic Parameters of the Oxidehydrogenation of Ethane with CO2 on Nanosized Calcium-Doped Ceria under Fast Deactivation Processes. *Catal. Today* **2006**, *112* (1), 148–152.
(13) Carrero, C. A.; Schloegl, R.; Wachs, I. E.; Schomaecker, R. Critical Literature Review of the Kinetics for the Oxidative Dehydrogenation of Propane over Well-Defined Supported Vanadium Oxide Catalysts. *ACS Catal.* **2014**, *4* (10), 3357–3380. https://doi.org/10.1021/cs5003417.
(14) Koirala, R.; Buechel, R.; Krumeich, F.; Pratsinis, S. E.; Baiker, A. Oxidative Dehydrogenation of Ethane with CO2 over Flame-Made Ga-Loaded TiO2. *ACS Catal.* **2015**, *5* (2), 690–702. https://doi.org/10.1021/cs500685d.
(15) Chen, K.; Khodakov, A.; Yang, J.; Bell, A. T.; Iglesia, E. Isotopic Tracer and Kinetic Studies of Oxidative Dehydrogenation Pathways on Vanadium Oxide Catalysts. *J. Catal.* **1999**, *186* (2), 325–333. https://doi.org/https://doi.org/10.1006/jcat.1999.2510.
(16) Chen, K.; Bell, A. T.; Iglesia, E. Kinetics and Mechanism of Oxidative Dehydrogenation of Propane on Vanadium, Molybdenum, and Tungsten Oxides. *J. Phys. Chem. B* **2000**, *104* (6), 1292–1299. https://doi.org/10.1021/jp9933875.
(17) Deng, S.; Li, S.; Li, H.; Zhang, Y. Oxidative Dehydrogenation of Ethane to Ethylene with CO2 over Fe−Cr/ZrO2 Catalysts. *Ind. Eng. Chem. Res.* **2009**, *48* (16), 7561–7566. https://doi.org/10.1021/ie9007387.
(18) Talati, A.; Haghighi, M.; Rahmani, F. Impregnation vs. Coprecipitation Dispersion of Cr over TiO2 and ZrO2 Used as Active and Stable Nanocatalysts in Oxidative Dehydrogenation of Ethane to Ethylene by Carbon Dioxide. *RSC Adv.* **2016**, *6* (50), 44195–44204. https://doi.org/10.1039/C6RA05049B.
(19) Nowicka, E.; Reece, C.; Althahban, S. M.; Mohammed, K. M. H.; Kondrat, S. A.; Morgan, D. J.; He, Q.; Willock, D. J.; Golunski, S.; Kiely, C. J.; et al. Elucidating the Role of CO2 in the Soft Oxidative Dehydrogenation of Propane over Ceria-Based Catalysts. *ACS Catal.* **2018**, *8* (4), 3454–3468. https://doi.org/10.1021/acscatal.7b03805.
(20) Gomez, E.; Yan, B.; Kattel, S.; Chen, J. G. Carbon Dioxide Reduction in Tandem with Light-Alkane Dehydrogenation. *Nat. Rev. Chem.* **2019**, *3* (11), 638–649. https://doi.org/10.1038/s41570-019-0128-9.
(21) Mukherjee, D.; Park, S.-E.; Reddy, B. M. CO2 as a Soft Oxidant for Oxidative Dehydrogenation Reaction: An Eco Benign Process for Industry. *J. CO2 Util.* **2016**, *16*, 301–312. https://doi.org/https://doi.org/10.1016/j.jcou.2016.08.005.
(22) Gionco, C.; Paganini, M. C.; Agnoli, S.; Reeder, A. E.; Giamello, E. Structural and Spectroscopic Characterization of CeO2–TiO2 Mixed Oxides. *J. Mater. Chem. A* **2013**, *1* (36), 10918–10926. https://doi.org/10.1039/C3TA12018J.
(23) Reddy, B. M.; Khan, A.; Yamada, Y.; Kobayashi, T.; Loridant, S.; Volta, J.-C. Structural Characterization of CeO2−MO2 (M = Si4+, Ti4+, and Zr4+) Mixed Oxides by Raman Spectroscopy, X-Ray Photoelectron Spectroscopy, and Other Techniques. *J. Phys. Chem. B* **2003**, *107* (41), 11475–11484. https://doi.org/10.1021/jp0358376.
(24) Dutta, G.; Waghmare, U. V; Baidya, T.; Hegde, M. S.; Priolkar, K. R.; Sarode, P. R. Origin of Enhanced Reducibility/Oxygen Storage Capacity of Ce1-XTixO2 Compared to CeO2 or TiO2. *Chem. Mater.* **2006**, *18* (14), 3249–3256. https://doi.org/10.1021/cm060267i.
(25) Shi, Z.; Yang, P.; Tao, F.; Zhou, R. New Insight into the Structure of CeO2–TiO2 Mixed Oxides and Their Excellent Catalytic Performances for 1,2-Dichloroethane Oxidation.

Chem. Eng. J. **2016**, *295*, 99–108. https://doi.org/https://doi.org/10.1016/j.cej.2016.03.032.
(26) Fang, J.; Bi, X.; Si, D.; Jiang, Z.; Huang, W. Spectroscopic Studies of Interfacial Structures of CeO2–TiO2 Mixed Oxides. *Appl. Surf. Sci.* **2007**, *253* (22), 8952–8961. https://doi.org/https://doi.org/10.1016/j.apsusc.2007.05.013.
(27) Watanabe, S.; Ma, X.; Song, C. Characterization of Structural and Surface Properties of Nanocrystalline TiO2−CeO2 Mixed Oxides by XRD, XPS, TPR, and TPD. *J. Phys. Chem. C* **2009**, *113* (32), 14249–14257. https://doi.org/10.1021/jp8110309.
(28) Reddy, B. M.; Khan, A.; Lakshmanan, P.; Aouine, M.; Loridant, S.; Volta, J.-C. Structural Characterization of Nanosized CeO2−SiO2, CeO2−TiO2, and CeO2−ZrO2 Catalysts by XRD, Raman, and HREM Techniques. *J. Phys. Chem. B* **2005**, *109* (8), 3355–3363. https://doi.org/10.1021/jp045193h.
(29) Tsilomelekis, G.; Tribalis, A.; Kalampounias, A. G.; Boghosian, S.; Panagiotou, G. D.; Bourikas, K.; Kordulis, C.; Lycourghiotis, A. Temperature – Dependent Evolution of Molecular Configurations of Oxomolybdenum Species on MoO3/TiO2 Catalysts Monitored by in Situ Raman Spectroscopy. In *Scientific Bases for the Preparation of Heterogeneous Catalysts*; Gaigneaux, E. M., Devillers, M., Hermans, S., Jacobs, P. A., Martens, J. A., Ruiz, P., Eds.; Studies in Surface Science and Catalysis; Elsevier, 2010; Vol. 175, pp 613–616. https://doi.org/https://doi.org/10.1016/S0167-2991(10)75120-X.
(30) Andriopoulou, C.; Boghosian, S. Heterogeneity of Deposited Phases in Supported Transition Metal Oxide Catalysts: Reversible Temperature-Dependent Evolution of Molecular Structures and Configurations. *Phys. Chem. Chem. Phys.* **2018**, *20* (3), 1742–1751. https://doi.org/10.1039/C7CP07286D.
(31) Xie, S.; Chen, K.; Bell, A. T.; Iglesia, E. Structural Characterization of Molybdenum Oxide Supported on Zirconia. *J. Phys. Chem. B* **2000**, *104* (43), 10059–10068. https://doi.org/10.1021/jp002419h.
(32) Hu, H.; Wachs, I. E.; Bare, S. R. Surface Structures of Supported Molybdenum Oxide Catalysts: Characterization by Raman and Mo L3-Edge XANES. *J. Phys. Chem.* **1995**, *99* (27), 10897–10910. https://doi.org/10.1021/j100027a034.
(33) Busca, G. Differentiation of Mono-Oxo and Polyoxo and of Monomeric and Polymeric Vanadate, Molybdate and Tungstate Species in Metal Oxide Catalysts by IR and Raman Spectroscopy. *J. Raman Spectrosc.* **2002**, *33* (5), 348–358. https://doi.org/10.1002/jrs.867.
(34) MESTL, G.; SRINIVASAN, T. K. K. Raman Spectroscopy of Monolayer-Type Catalysts: Supported Molybdenum Oxides. *Catal. Rev.* **1998**, *40* (4), 451–570. https://doi.org/10.1080/01614949808007114.
(35) Bañares, M. A.; Wachs, I. E. Molecular Structures of Supported Metal Oxide Catalysts under Different Environments. *J. Raman Spectrosc.* **2002**, *33* (5), 359–380. https://doi.org/10.1002/jrs.866.
(36) Tsilomelekis, G.; Panagiotou, G. D.; Stathi, P.; Kalampounias, A. G.; Bourikas, K.; Kordulis, C.; Deligiannakis, Y.; Boghosian, S.; Lycourghiotis, A. Molybdena Deposited on Titania by Equilibrium Deposition Filtration: Structural Evolution of Oxo–molybdenum(vi) Sites with Temperature. *Phys. Chem. Chem. Phys.* **2016**, *18* (34), 23980–23989. https://doi.org/10.1039/C6CP05247A.
(37) Liu, H.; Cheung, P.; Iglesia, E. Structure and Support Effects on the Selective Oxidation of Dimethyl Ether to Formaldehyde Catalyzed by MoOx Domains. *J. Catal.* **2003**, *217* (1), 222–232. https://doi.org/https://doi.org/10.1016/S0021-9517(03)00025-3.
(38) Vuurman, M. A.; Wachs, I. E. In Situ Raman Spectroscopy of Alumina-Supported Metal

Oxide Catalysts. *J. Phys. Chem.* **1992**, *96* (12), 5008–5016. https://doi.org/10.1021/j100191a051.
(39) Radhakrishnan, R.; Reed, C.; Oyama, S. T.; Seman, M.; Kondo, J. N.; Domen, K.; Ohminami, Y.; Asakura, K. Variability in the Structure of Supported MoO3 Catalysts: Studies Using Raman and X-Ray Absorption Spectroscopy with Ab Initio Calculations. *J. Phys. Chem. B* **2001**, *105* (36), 8519–8530. https://doi.org/10.1021/jp0117361.
(40) Weckhuysen, B. M.; Jehng, J.-M.; Wachs, I. E. In Situ Raman Spectroscopy of Supported Transition Metal Oxide Catalysts: 18O2−16O2 Isotopic Labeling Studies. *J. Phys. Chem. B* **2000**, *104* (31), 7382–7387. https://doi.org/10.1021/jp000055n.
(41) Burcham, L. J.; Datka, J.; Wachs, I. E. In Situ Vibrational Spectroscopy Studies of Supported Niobium Oxide Catalysts. *J. Phys. Chem. B* **1999**, *103* (29), 6015–6024. https://doi.org/10.1021/jp990289a.
(42) Wachs, I. E. In Situ Raman Spectroscopy Studies of Catalysts. *Top. Catal.* **1999**, *8* (1), 57–63. https://doi.org/10.1023/A:1019100925300.
(43) Watson, R. B.; Ozkan, U. S. Mo Loading Effects over Mo/Si : Ti Catalysts in the Oxidative Dehydrogenation of Ethane. *J. Catal.* **2002**, *208* (1), 124–138. https://doi.org/https://doi.org/10.1006/jcat.2002.3548.
(44) Dai, H.; Bell, A. T.; Iglesia, E. Effects of Molybdena on the Catalytic Properties of Vanadia Domains Supported on Alumina for Oxidative Dehydrogenation of Propane. *J. Catal.* **2004**, *221* (2), 491–499. https://doi.org/https://doi.org/10.1016/j.jcat.2003.09.020.
(45) Chen, K.; Xie, S.; Iglesia, E.; Bell, A. T. Structure and Properties of Zirconia-Supported Molybdenum Oxide Catalysts for Oxidative Dehydrogenation of Propane. *J. Catal.* **2000**, *189* (2), 421–430. https://doi.org/https://doi.org/10.1006/jcat.1999.2720.
(46) Tsilomelekis, G.; Boghosian, S. An Operando Raman Study of Molecular Structure and Reactivity of Molybdenum(vi) Oxide Supported on Anatase for the Oxidative Dehydrogenation of Ethane. *Phys. Chem. Chem. Phys.* **2012**, *14* (7), 2216–2228. https://doi.org/10.1039/C1CP22586C.
(47) Samek, I. A.; Bobbitt, N. S.; Snurr, R. Q.; Stair, P. C. Structure and Activity of Mixed VOx-CeO2 Domains Supported on Alumina in Cyclohexane Oxidative Dehydrogenation. *J. Catal.* **2020**, *384*, 147–158. https://doi.org/https://doi.org/10.1016/j.jcat.2020.02.017.
(48) Ruiz Puigdollers, A.; Schlexer, P.; Tosoni, S.; Pacchioni, G. Increasing Oxide Reducibility: The Role of Metal/Oxide Interfaces in the Formation of Oxygen Vacancies. *ACS Catal.* **2017**, *7* (10), 6493–6513. https://doi.org/10.1021/acscatal.7b01913.
(49) Baidya, T.; Gayen, A.; Hegde, M. S.; Ravishankar, N.; Dupont, L. Enhanced Reducibility of Ce1-XTixO2 Compared to That of CeO2 and Higher Redox Catalytic Activity of Ce1-x-YTixPtyO2-δ Compared to That of Ce1-XPtxO2-δ. *J. Phys. Chem. B* **2006**, *110* (11), 5262–5272. https://doi.org/10.1021/jp0565103.
(50) Zhou, R.; Cao, Y.; Yan, S.; Fan, K. Rare Earth (Y, La, Ce)-Promoted V-HMS Mesoporous Catalysts for Oxidative Dehydrogenation of Propane. *Appl. Catal. A Gen.* **2002**, *236* (1), 103–111. https://doi.org/https://doi.org/10.1016/S0926-860X(02)00281-8.
(51) Olthof, B.; Khodakov, A.; Bell, A. T.; Iglesia, E. Effects of Support Composition and Pretreatment Conditions on the Structure of Vanadia Dispersed on SiO2, Al2O3, TiO2, ZrO2, and HfO2. *J. Phys. Chem. B* **2000**, *104* (7), 1516–1528. https://doi.org/10.1021/jp9921248.
(52) Yan, B.; Yao, S.; Kattel, S.; Wu, Q.; Xie, Z.; Gomez, E.; Liu, P.; Su, D.; Chen, J. G. Active Sites for Tandem Reactions of CO2 Reduction and Ethane Dehydrogenation. *Proc. Natl.*

Acad. Sci. **2018**, *115* (33), 8278–8283. https://doi.org/10.1073/pnas.1806950115.
(53) Christodoulakis, A.; Heracleous, E.; Lemonidou, A. A.; Boghosian, S. An Operando Raman Study of Structure and Reactivity of Alumina-Supported Molybdenum Oxide Catalysts for the Oxidative Dehydrogenation of Ethane. *J. Catal.* **2006**, *242* (1), 16–25. https://doi.org/https://doi.org/10.1016/j.jcat.2006.05.024.
(54) GeorgeTsilomelekis, S.; Boghosian. Structural and Vibrational Properties of Molybdena Catalysts Supported on Alumina and Zirconia Studied by in Situ Raman and FTIR Spectroscopies Combined with 18O/16O Isotopic Substitution. *Catal. Today* **2010**, *158* (1), 146–155.